

RENDICONTI LINCEI MATEMATICA E APPLICAZIONI

ALBERTO CARPINTERI

Cohesive crack tip modelling: size-scale transition from ductile to brittle failure

Atti della Accademia Nazionale dei Lincei. Classe di Scienze Fisiche, Matematiche e Naturali. Rendiconti Lincei. Matematica e Applicazioni, Serie 9, Vol. 1 (1990), n.1, p. 59–79.

Accademia Nazionale dei Lincei

<http://www.bdim.eu/item?id=RLIN_1990_9_1_1_59_0>

L'utilizzo e la stampa di questo documento digitale è consentito liberamente per motivi di ricerca e studio. Non è consentito l'utilizzo dello stesso per motivi commerciali. Tutte le copie di questo documento devono riportare questo avvertimento.

Atti della Accademia Nazionale dei Lincei. Classe di Scienze Fisiche, Matematiche e Naturali. Rendiconti Lincei. Matematica e Applicazioni, Accademia Nazionale dei Lincei, 1990.

Meccanica dei solidi. — *Cohesive crack tip modelling: size-scale transition from ductile to brittle failure.* Nota di ALBERTO CARPINTERI, presentata (*) dal Corrisp. G. MAIER.

ABSTRACT. — The nature of the crack and the structure behaviour can range from ductile to brittle depending on tensile strength and fracture toughness of the material, as well as on the size-scale of the solid body. Strength and toughness present in fact different physical dimensions and any consistent fracture criterion must consider energy dissipation both per unit of volume and per unit of crack area. A cohesive crack model is proposed aiming at describing the size effects of fracture mechanics, *i.e.*, the transition from ductile to brittle global behaviour caused by increasing the size-scale and keeping the geometrical shape unchanged. For extremely brittle cases (*e.g.*, initially uncracked specimens, large and/or slender structures, low fracture toughness, high tensile strength, etc.) a snap-back instability in the load-deflection path occurs. If the loading process is deflection-controlled, the loading capacity presents a discontinuity with a negative jump. It is proved that such a catastrophic event tends to reproduce the classical LEFM-instability ($K_I = K_{IC}$).

KEY WORDS: Fracture mechanics; Ductility; Brittleness; Dimensional effects; Brittleness number.

RIASSUNTO. — *Modello della fessura con forze coesive: transizione dimensionale tra rottura duttile e fragile.* Il comportamento di una fessura e del solido che la contiene può variare da duttile a fragile, in funzione della resistenza alla trazione e della tenacità alla frattura del materiale, così come delle dimensioni del solido stesso. Resistenza e tenacità presentano infatti dimensioni fisiche diverse, e un criterio di rottura coerente dovrebbe prevedere dissipazione energetica sia nell'unità di volume del solido che sull'unità di superficie della fessura che si forma. Nella presente nota si propone un modello matematico della fessura dotato di forze coesive, le quali simulano gli effetti plastici e permettono di descrivere la transizione duttile-fragile che si verifica all'aumentare delle dimensioni strutturali, pur mantenendo invariata la forma geometrica del solido. Per casi di estrema fragilità (es., solidi cristallini, strutture grandi e/o snelle, basse tenacità alla frattura, alte resistenze alla trazione), si evidenzia un fenomeno di instabilità catastrofica nel diagramma forza-spostamento. Se il processo di caricamento avviene imponendo una crescita monotona allo spostamento, la capacità portante in funzione dello spostamento mostrerà una discontinuità con un salto negativo. Si verifica che tale evento tende a riprodurre la ormai classica instabilità della Meccanica della Frattura Elastica Lineare ($K_I = K_{IC}$).

1. INTRODUCTION

The cohesive crack model is a representative model when the plastic zone is confined to a very narrow band. The plastic stress field is represented by restraining forces which close the crack tip faces. These forces are non-increasing functions of the distance between the crack surfaces.

Such a model was originally proposed by Barenblatt [1], who considered the cohesive forces confined to an interaction zone of constant size, with the shape of the terminal crack region being fixed even if translating. On the other hand, Dugdale [9] considered a similar model with vanishing singularity at the crack tip and an interaction zone of variable size, spreading into the entire ligament at the condition of general yielding.

(*) Nella seduta dell'11 marzo 1989.

In the following years the cohesive crack model was reconsidered, with some modifications, by several Authors: Bilby, Cottrell and Swinden [3], Rice [13], Wnuk [18], Hillerborg, Modeer and Petersson [11], etc.

In the present paper the cohesive crack model is applied to analyse the stable *vs.* unstable crack propagation in elastic-softening materials. The crack propagation in real structures often presents a transition from slow to fast rate, and viceversa. In other cases the crack propagation is only slow or fast. This happens in dependence on material properties, structure geometry, loading condition and external constraints. The influence of variation in fracture toughness, tensile strength and geometrical size-scale will be investigated on the basis of the π -Theorem of dimensional analysis ([5], [6], [8]). Strength and toughness present in fact different physical dimensions and any consistent failure criterion must describe energy dissipation per unit of volume and per unit of crack area respectively.

For extremely brittle cases (*e.g.*, initially uncracked specimens, large and/or slender elements, low fracture toughness, high tensile strength, etc.) a snap-back instability appears in the load-displacement curve, which presents a softening branch with positive slope. This means that both load and deflection must decrease to obtain a slow and controlled crack propagation, whereas in normal softening (negative slope) only the load must decrease. If, at the snap-back instability, the loading process is displacement-controlled, the load *vs.* displacement path will present a negative jump onto the lower branch with negative slope.

The accuracy of the numerical description of cohesive crack propagation is also investigated. It is shown that, when the finite element mesh is too coarse, *i.e.*, when the cohesive forces are too far one from the other, the cohesive model is unable to describe fracture process and mechanical behaviour regularly. In other words, when the structure is very large or the fracture toughness very small, the plastic or cohesive zone at the crack tip becomes relatively small, and the finite element mesh must be refined, so that such a zone and the LEFM-stress-singularity may be properly reproduced and the snap-back instability described even in the post-peak and post-catastrophical stage.

The snap-back instability was studied in the past by several Authors: Maier [12], Bazant [2], Carpinteri [8], Schreyer [16], Rots *et al.* [15], etc. On the other hand, the object of the present paper is to put it in connection with the LEFM-instability. From an experimental point of view, the snap-back instability was originally detected by Fairhurst *et al.* [10] in the compressive behaviour of rocks and more recently by Rokugo *et al.* [14] and Biolzi *et al.* [4] in the bending behaviour of concrete.

2. STRAIN-SOFTENING INSTABILITY OF SLAB IN TENSION

Let us consider an elastic-softening material with a double constitutive law: (*a*) tension σ *vs.* dilatation ε , and (*b*) tension σ *vs.* crack opening displacement w , after reaching the ultimate tensile strength σ_u or strain $\varepsilon_u = \sigma_u/E$ (fig. 1):

$$(1-a) \quad \sigma = E\varepsilon, \quad \text{for } \varepsilon \leq \varepsilon_u,$$

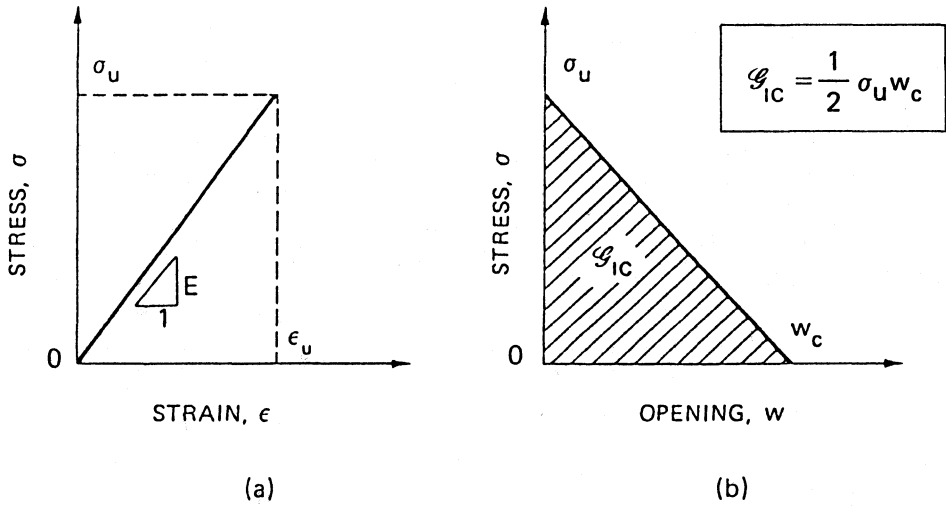


Fig. 1. - (a) Stress-strain; (b) linear stress-crack opening displacement law.

$$\begin{aligned}
 (1-b) \quad & \sigma = \sigma_u (1 - w/w_c), & \text{for } w \leq w_c, \\
 (1-c) \quad & \sigma = 0, & \text{for } w > w_c.
 \end{aligned}$$

According to eq. (1-c), the cohesive interaction between the crack surfaces vanishes for distances larger than the critical opening w_c .

If a plane slab is increasingly loaded, the deformation history will undergo three different stages.

(A) The slab behaves elastically without damage or fracture zones (fig. 2a). The

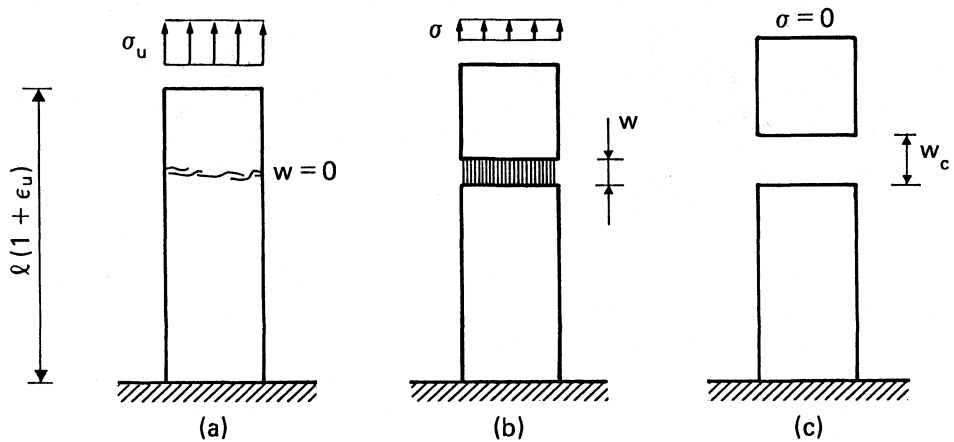


Fig. 2. - Stages of the deformation history. (a) Elastic behaviour; (b) strain-softening behaviour; (c) complete separation.

displacement of the upper edge is:

$$(2) \quad \delta = (\sigma/E)l, \quad \text{for } \varepsilon \leq \varepsilon_u.$$

(B) After reaching the ultimate tensile strength σ_u , a fracture cohesive zone develops in the weakest section of the slab. Observe that, as the stress field is homogeneous, another cause of non-homogeneity must be assumed for strain-localization. The slab behaves elastically only outside the fracture zone (fig. 2*b*). The displacement of the upper edge is:

$$(3) \quad \delta = (\sigma/E)l + w, \quad \text{for } w \leq w_c.$$

Recalling eq. (1-*b*), eq. (3) gives:

$$(4) \quad \delta = (\sigma/E)l + w_c(1 - \sigma/\sigma_u), \quad \text{for } w \leq w_c.$$

While the fracture zone opens, the elastic zone shrinks at progressively decreasing stresses. At this stage, the loading process may be stable only if it is displacement-controlled, *i.e.*, if the external displacement δ is imposed. But this is only a necessary and not sufficient condition for stability.

(C) When $\delta \geq w_c$ the reacting stress σ vanishes, the cohesive forces disappear and the slab is completely separated into two pieces (fig. 2*c*).

Rearranging of eq. (2) gives:

$$(5) \quad \sigma = E\delta/l, \quad \text{for } \delta \leq \varepsilon_u l,$$

while the condition of complete separation (stage C) reads:

$$(6) \quad \sigma = 0, \quad \text{for } \delta \geq w_c.$$

When $w_c > \varepsilon_u l$, the softening process is stable only if displacement-controlled, since the slope $d\sigma/d\delta$ at stage (B) is negative (fig. 3*a*). When $w_c = \varepsilon_u l$, the slope $d\sigma/d\delta$ is infinite and a drop in the loading capacity occurs, even if the loading is displacement-controlled (fig. 3*b*). Eventually, when $w_c < \varepsilon_u l$, the slope $d\sigma/d\delta$ becomes positive (fig. 3*c*) and the same negative jump occurs like that shown in fig. 3*b*.

Rearranging of eq. (4) provides:

$$(7) \quad \delta = w_c + \sigma(l/E - w_c/\sigma_u).$$

The same conditions just obtained from a geometrical point of view (fig. 3), may also be given by the analytical derivation of eq. (7).

Normal softening occurs for $d\delta/d\sigma < 0$:

$$(8) \quad (l/E - w_c/\sigma_u) < 0,$$

whereas catastrophic softening (snap-back) for $d\delta/d\sigma \geq 0$:

$$(9) \quad (l/E - w_c/\sigma_u) \geq 0.$$

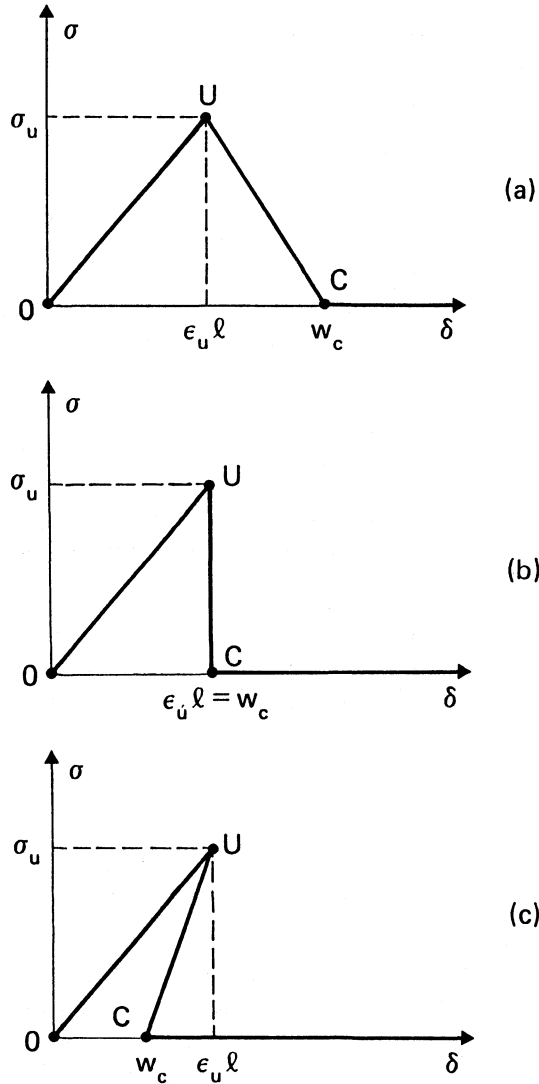


Fig. 3. – Elastic-softening global behaviour. (a) Normal softening; (b) vertical drop in the loading capacity; (c) catastrophical softening (or snap-back).

Eq. (9) may be rearranged in the following form:

$$(10) \quad (\omega_c/2b) [\epsilon_u(l/b)]^{-1} \leq 1/2,$$

where b is the slab width.

The ratio $(\omega_c/2b)$ is a dimensionless number, which is a function of material properties and structural size-scale, [8]:

$$(11) \quad s_E = \omega_c/2b = \mathcal{G}_{IC}/\sigma_u b,$$

$\mathcal{G}_{IC} = \sigma_u \omega_c / 2$ being the fracture energy of the material (fig. 1). The brittleness number s_E describes the scale effects of fracture mechanics, *i.e.*, the ductile-brittle transition when the size-scale is increased. Eq. (10) may be presented in the following final form:

$$(12) \quad s_E / \varepsilon_u \lambda \leq 1/2,$$

with $\lambda = \text{slenderness} = l/b$.

When the size-scale and the slab slenderness are relatively large and the fracture energy relatively low, the global structural behaviour is brittle. Not the single values of parameters s_E , ε_u and λ , but only their combination $B = s_E / \varepsilon_u \lambda$ is responsible for the global brittleness or ductility of the structure considered.

When $B \leq 1/2$, the plane rectangular slab of fig. 2 shows a mechanical behaviour which can be defined *brittle* or *catastrophic*. A *bifurcation* or *branching* of the global equilibrium occurs, since, if point *U* in fig. 3c is reached and then the imposed external displacement δ is decreased by a very small amount $d\delta$, the global unloading may occur along two alternative paths: the elastic UO or the virtual softening UC.

The global brittleness of the slab can be defined as the ratio of the ultimate elastic energy contained in the body to the energy dissipated by fracture:

$$(13) \quad \text{Brittleness} = [(\sigma_u^2 / 2E) \times (\text{Area}) \times l] \times [\mathcal{G}_{IC} \times (\text{Area})]^{-1} = 1/2B.$$

Such a ratio is higher than unity when eq. (9) is verified and a catastrophic softening instability occurs.

3. COHESIVE CRACK MODEL AND DUCTILE-BRITTLE TRANSITION

The cohesive crack model is based on the following assumptions [11,8].

(1) The cohesive fracture zone (plastic or process zone) begins to develop when the maximum principal stress achieves the ultimate tensile strength σ_u (fig. 1a).

(2) The material in the process zone is partially damaged but still able to transfer stress. Such a stress is dependent on the crack opening displacement ω (fig. 1b).

The *real crack tip* is defined as the point where the distance between the crack surfaces is equal to the critical value of crack opening displacement ω_c and the normal stress vanishes (fig. 4a). On the other hand, the *fictitious crack tip* is defined as the point where the normal stress attains the maximum value σ_u and the crack opening vanishes (fig. 4a).

The closing stresses acting on the crack surfaces (fig. 4a) can be replaced by nodal forces (fig. 4b). The intensity of these forces depends on the opening of the fictitious crack, ω , according to the σ - ω constitutive law of the material (fig. 1b). When the tensile strength σ_u is achieved at the fictitious crack tip (fig. 4b), the top node is opened and a cohesive force starts acting across the crack, while the fictitious crack tip moves to the next node.

With reference to the three point bending test (TPBT) geometry in fig. 5, the nodes are distributed along the potential fracture line.

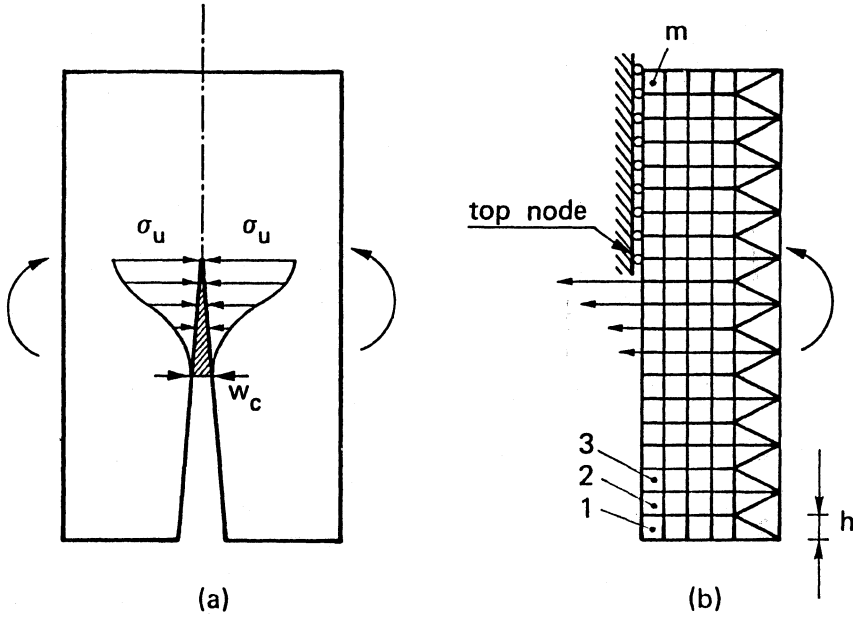


Fig. 4. – (a) Stress distribution across the cohesive zone and (b) equivalent nodal forces in the finite element mesh.

The coefficients of influence in terms of node openings and deflection are computed by a finite element analysis where the fictitious structure in fig. 5 is subjected to $(n + 1)$ different loading conditions. Consider the TPBT in fig. 6a with the initial crack of length a_0 and tip in the node k . The crack opening displacements at the n fracture nodes may be expressed as follows:

$$(14) \quad \omega = KF + CP + \Gamma$$

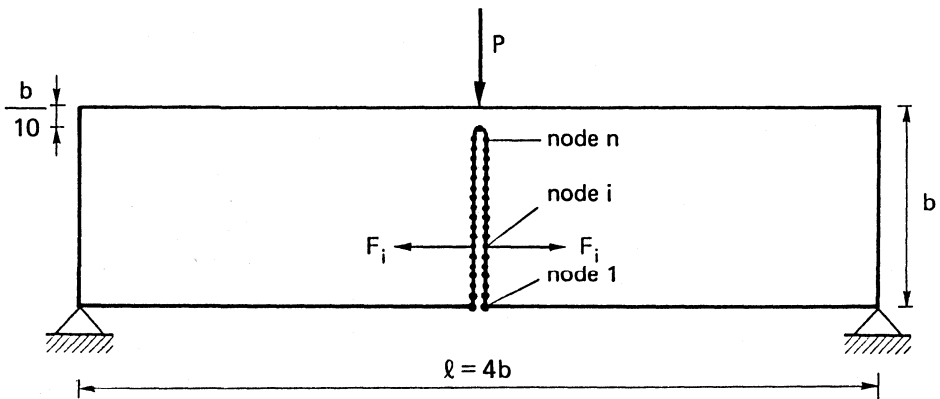


Fig. 5. – Finite element nodes along the potential fracture line.

being:

- w = vector of the crack opening displacements,
- K = matrix of the coefficients of influence (nodal forces),
- F = vector of the nodal forces,
- C = vector of the coefficients of influence (external load),
- P = external load,
- Γ = vector of the crack opening displacements due to the specimen weight.

On the other hand, the initial crack is stress-free and therefore:

$$(15-a) \quad F_i = 0, \quad \text{for } i = 1, 2, \dots, (k-1),$$

while at the ligament there is no displacement discontinuity:

$$(15-b) \quad w_i = 0, \quad \text{for } i = k, (k+1), \dots, n.$$

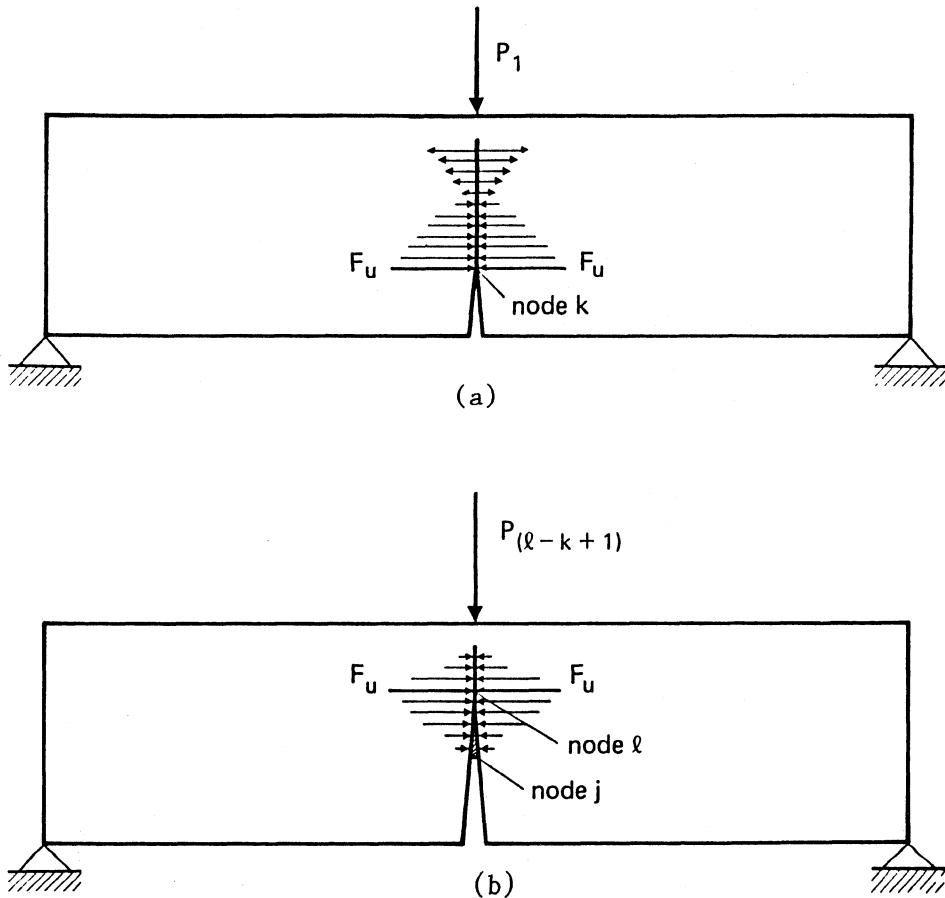


Fig. 6. - Cohesive crack configurations at the first (a) and $(l-k+1)$ -th (b) crack growth increment.

Eqs. (14) and (15) constitute a linear algebraical system of $2n$ equations and $2n$ unknowns, *i.e.*, the elements of vectors \boldsymbol{w} and \boldsymbol{F} . If load P and vector \boldsymbol{F} are known, it is possible to compute the beam deflection, δ :

$$(16) \quad \delta = \mathbf{C}^T \mathbf{F} + D_p P + D_\gamma,$$

where D_p is the deflection for $P = 1$ and D_γ is the deflection due to the specimen weight.

After the first step, a cohesive zone forms in front of the real crack tip (fig. 6*b*), say between nodes j and l . Then eqs. (2) are replaced by:

$$(17-a) \quad F_i = 0, \quad \text{for } i = 1, 2, \dots, (j - 1),$$

$$(17-b) \quad F_i = F_u(1 - w_i / w_c), \quad \text{for } i = j, (j + 1), \dots, l,$$

$$(17-c) \quad w_i = 0, \quad \text{for } i = l, (l + 1), \dots, n,$$

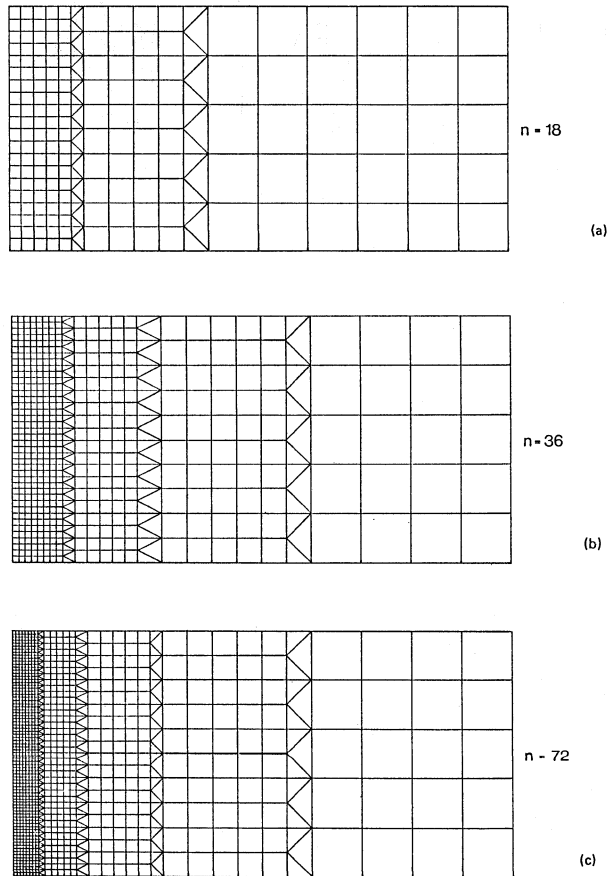


Fig. 7. - Refinement of the finite element mesh.

where F_u is the ultimate strength nodal force:

$$(18) \quad F_u = b\sigma_u/m.$$

Eqs. (14) and (17) constitute a linear algebraical system of $(2n + 1)$ equations and $(2n + 1)$ unknowns, *i.e.*, the elements of vector ω and F and the external load P .

The present numerical program simulates a loading process where the controlling parameter is the fictitious crack depth. On the other hand, real (or stress-free) crack depth, external load and deflection are obtained at each step after an iterative procedure.

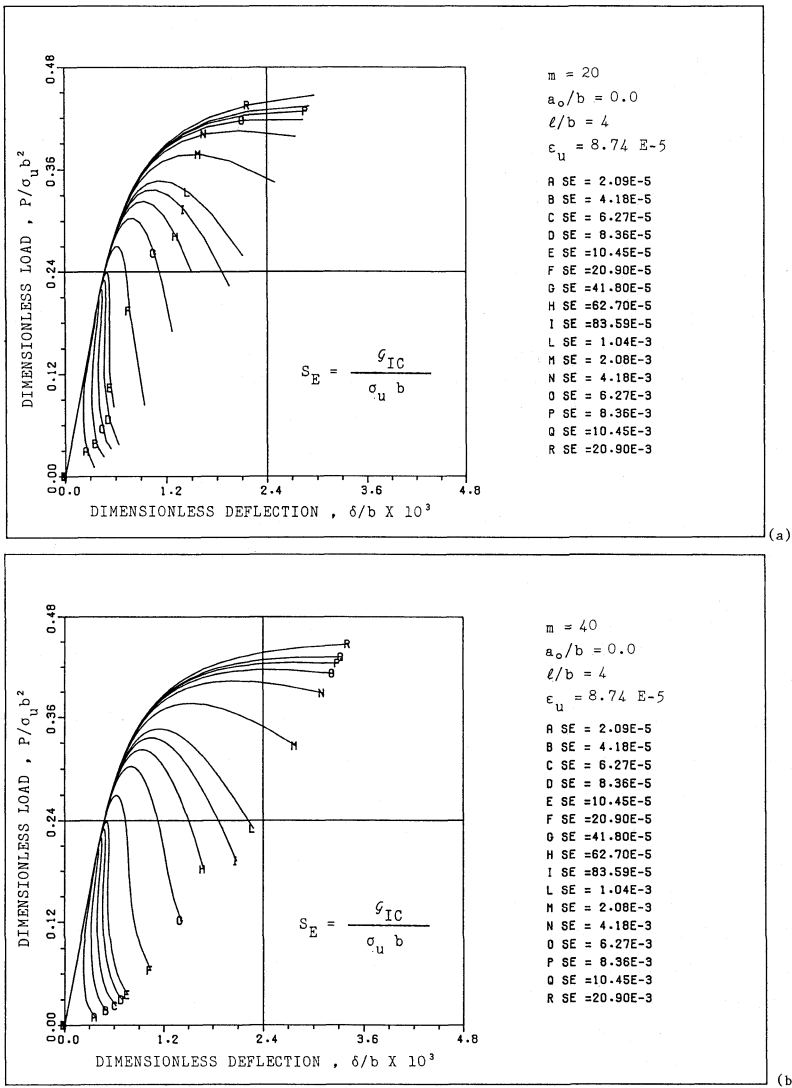


Fig. 8. - Dimensionless load-deflection response of an initially uncracked specimen, by varying the brittleness number, $s_E = G_{IC}/\sigma_u b = \omega_c/2b$, between 2×10^{-5} and 2×10^{-2} . (a) $m = 20$, (b) $m = 40$, (c) $m = 80$.

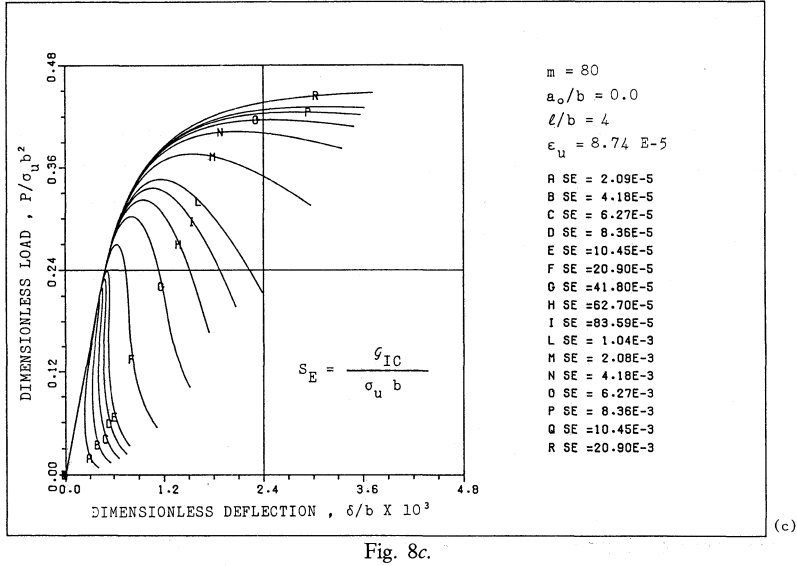


Fig. 8c.

The three point bending beam in fig. 5 is considered herein, with the constant geometrical proportions: span = $l = 4b$, thickness = $t = b$. The scale factor is therefore represented by the beam depth b .

As is shown in fig. 4b, m finite elements are adjacent to the central line, whereas only $n = 0.9 m$ nodes can be untied during the crack growth (fig. 5). The finite element size h (fig. 4b) is then connected with the beam depth b through the simple relation: $b = mb$.

The three different finite element meshes in fig. 7 are considered. Mesh (a) presents 20 elements and 18 fracture nodes, mesh (b) 40 elements and 36 fracture nodes, mesh (c) 80 elements and 72 fracture nodes.

The load-deflection response of the three point bending beam in fig. 5 is represented in figs. 8a, b and c, for $m = 20, 40$ and 80 respectively. The initial crack depth is assumed $a_0/b = 0.0$, while the ultimate tensile strain $\epsilon_u = \sigma_u/E$ is 8.7×10^{-5} and the Poisson ratio $\nu = 0.1$. The diagrams are plotted in non-dimensional form by varying the brittleness number s_E . The simple variation in this dimensionless number reproduces all the cases related to the independent variations in G_{IC} , b and σ_u . Not the single values of G_{IC} , b and σ_u , but their function s_E —see eq. (11)—is responsible for the structural behaviour, which can range from ductile to brittle. Specimens with high fracture toughness are then ductile, as well as small specimens and/or specimens with low tensile strength. Vice versa, brittle behaviours are predicted for low fracture toughnesses, large specimens and/or high tensile strengths.

The influence of the variation in the number s_E is investigated over four orders of magnitude in figs. 8, from 2×10^{-2} to 2×10^{-5} . The results reported in figs. 8a, b and c, appear very similar. Of course, the diagrams for $m = 20$ (fig. 8a) are slightly less regular than those for $m = 80$ (fig. 8c), and present some weak cuspidal points especially for low s_E numbers.

When ulteriorly lower s_E numbers are contemplated, the $P-\delta$ diagrams lose their regularity, from a mathematical point of view, and their resolution, from a graphical point of view. The influence of the variation in the s_E number is further analyzed over one order of magnitude in fig. 9, from 2×10^{-5} to 2×10^{-6} . The results reported in figs. 9a, b and c appear much less uniform than those in figs. 8a, b and c. The diagrams for $m = 20$ (fig. 9a) are lacking in mathematical regularity, graphical resolution and physical meaning. The diagrams present a slightly better regularity and resolution for $m = 40$ (fig. 9b), whereas, for $m = 80$ (fig. 9c), they appear sufficiently regular,

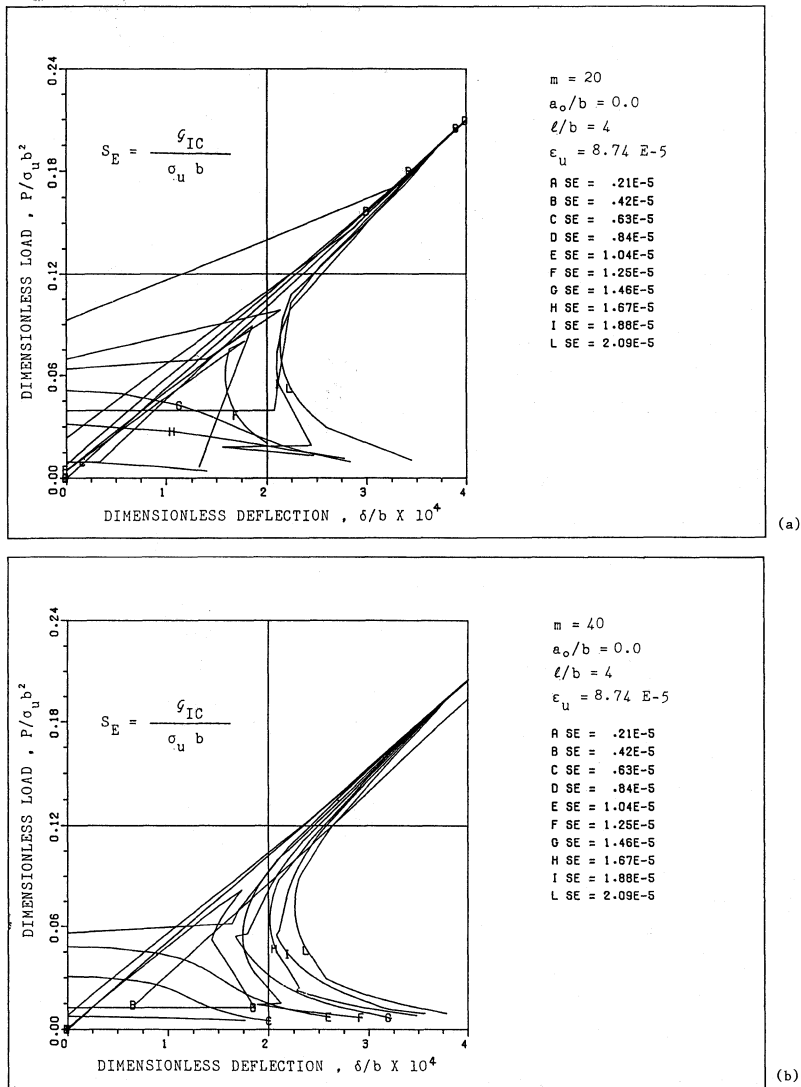


Fig. 9. – Dimensionless load-deflection response of an initially uncracked specimen, by varying the brittleness number, $s_E = G_{IC}/\sigma_u b = w_c/2b$, between 2×10^{-6} and 2×10^{-5} . (a) $m = 20$, (b) $m = 40$, (c) $m = 80$.

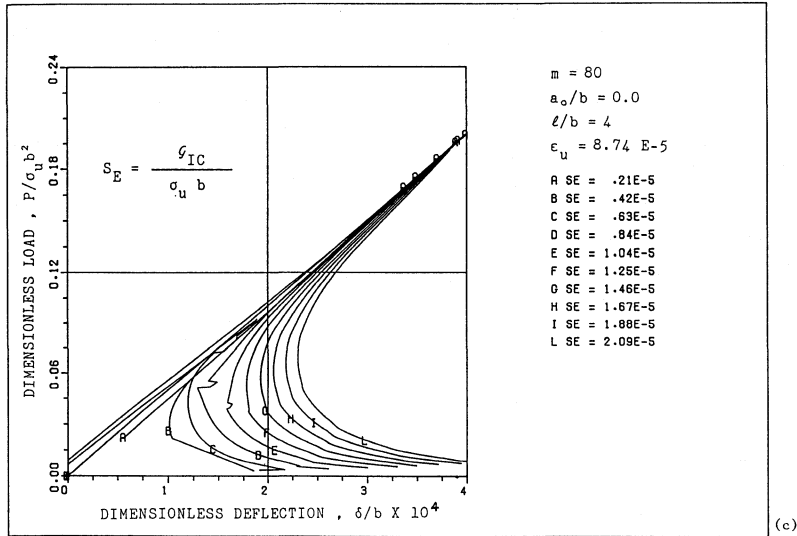


Fig. 9c.

especially for not too low brittleness numbers ($10^{-5} \leq s_E \leq 2 \times 10^{-5}$). If a better resolution is requested for $2 \times 10^{-6} \leq s_E \leq 10^{-5}$, the mesh must be refined, *i.e.*, the number m increased. On the other hand, it is evident that the mesh must be refined, *i.e.*, the cohesive forces must be closer, for relatively large structures and/or for relatively brittle materials, where the cohesive zone is confined to a relatively small crack tip region.

From the cases shown in figs. 8 and 9, the s_E -threshold below which the results are

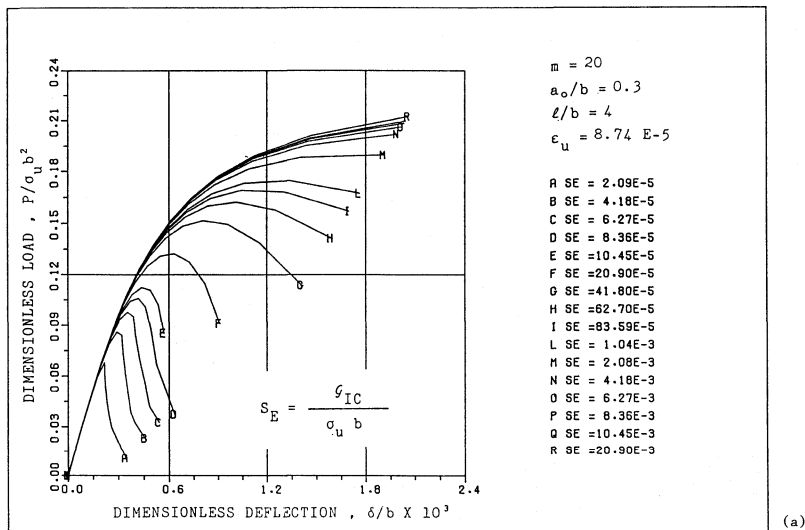


Fig. 10. – Dimensionless load-deflection response of an initially cracked specimen ($a_0/b = 0.3$), by varying the brittleness number, $s_E = G_{IC}/\sigma_u b = w_c/2b$, between 2×10^{-5} and 2×10^{-2} . (a) $m = 20$, (b) $m = 40$, (c) $m = 80$.

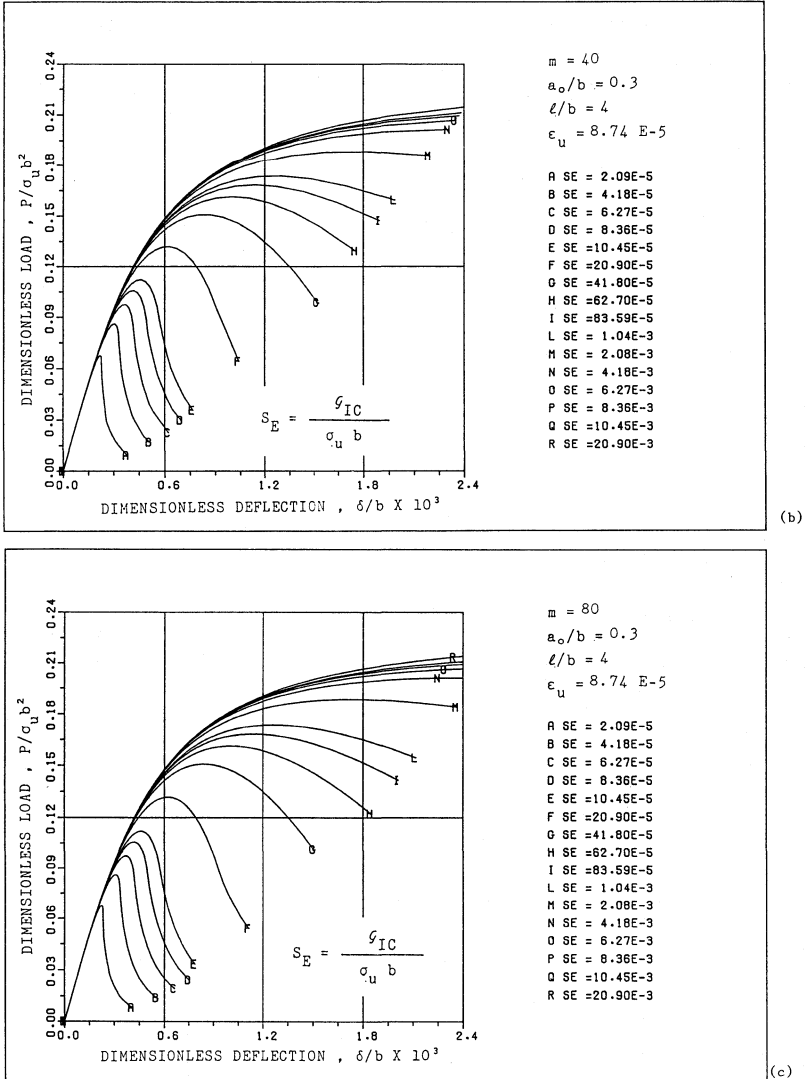


Fig. 10b-c.

unacceptable results to be approximately:

$$(19) \quad s_E = \omega_c / 2mb \approx (80/m) \times 10^{-5}.$$

The lower bound to s_E can be regarded as an upper bound to the finite element size b :

$$(20) \quad b \leq 600 \omega_c.$$

For a concrete-like material with maximum aggregate size of 2 cm, it is approximately $\omega_c \approx 0.1$ mm and then eq. (20) provides: $b \leq 6$ cm.

The load-deflection response shows the same trends even when an initial crack is present in the lower edge of the three point bending beam. The initial crack depth is

considered to be $a_0/b = 0.3$ (figs. 10 and 11). The deeper the initial crack is, the more ductile the beam behaviour results.

In addition to the slenderness $l/b = 4$ considered so far, the ratios $l/b = 8$ and 16 are then contemplated. For initially uncracked specimens ($a_0/b = 0.0$), fig. 8b ($l/b = 4$) is to be compared with fig. 12a ($l/b = 8$) and fig. 12b ($l/b = 16$). The brittleness increase with the slab slenderness is manifest.

Such a trend is due to the variation in the elastic compliance of the non-damaged

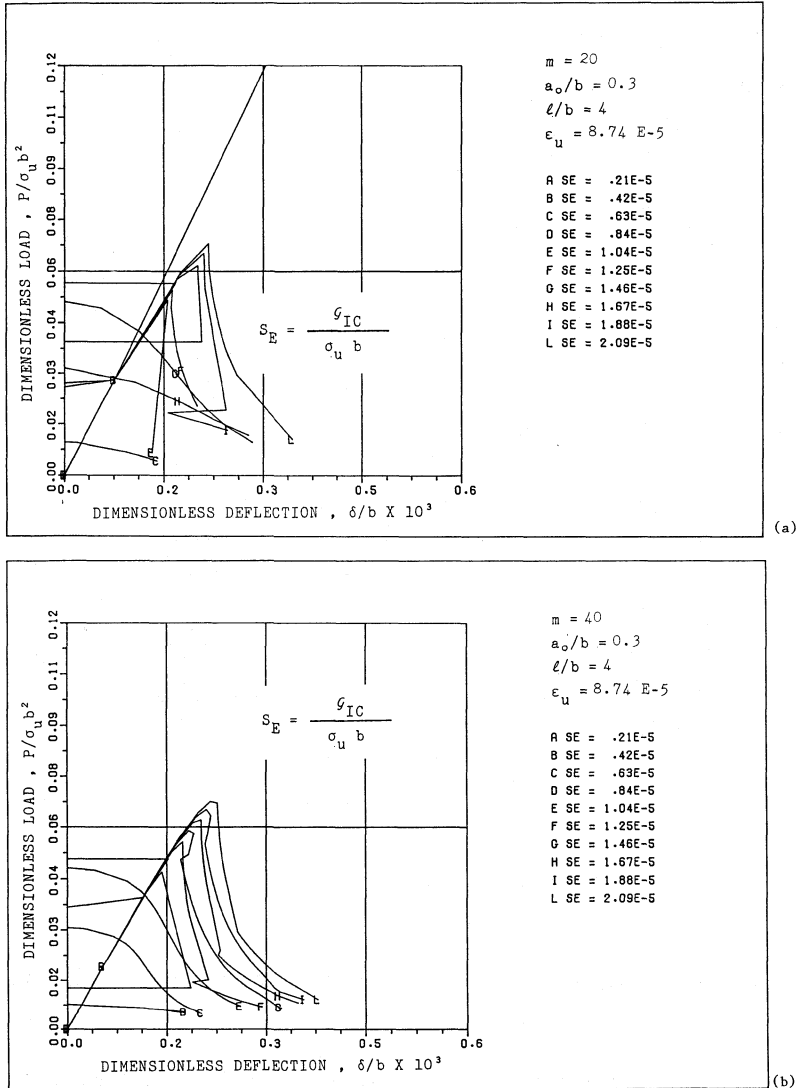


Fig. 11. – Dimensionless load-deflection response of an initially cracked specimen ($a_0/b = 0.3$) by varying the brittleness number, $s_E = G_{IC}/\sigma_u b = \omega_c/2b$, between 2×10^{-6} and 2×10^{-5} . (a) $m = 20$, (b) $m = 40$, (c) $m = 80$.

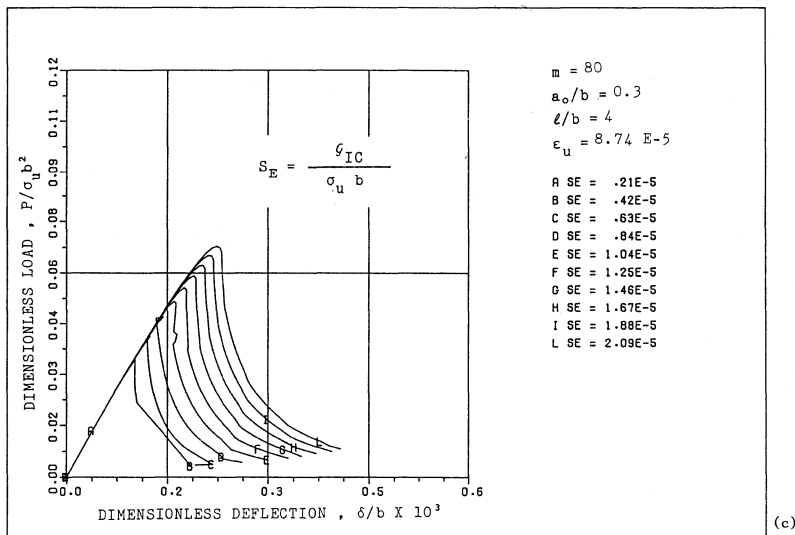


Fig. 11c.

zone. An increase of this compliance produces an increase of brittleness in the system. In the softening stage, in fact, the elastic recovery prevails over the localized increase of deformation, so that a snap-back instability occurs (see section 2).

4. SIZE-SCALE EFFECTS: DECREASE OF APPARENT STRENGTH AND INCREASE OF FICTITIOUS FRACTURE TOUGHNESS

The maximum loading capacity $P_{\max}^{(1)}$ of initially uncracked specimens with $l = 4b$ is obtained from figs. 8 and 9. On the other hand, the maximum load $P_{\max}^{(3)}$ of ultimate strength is given by:

$$(21) \quad P_{\max}^{(3)} = 2\sigma_u t b^2 / 3l.$$

The values of the ratio $P_{\max}^{(1)} / P_{\max}^{(3)}$ may also be regarded as the ratio of the apparent tensile strength σ_f (given by the maximum load $P_{\max}^{(1)}$ and applying eq. (21)) to the true tensile strength σ_u (considered as a material constant). It is evident from fig. 13 that the results of the cohesive crack model tend to those of the ultimate strength analysis for low s_E values:

$$(22) \quad \lim_{s_E \rightarrow 0} P_{\max}^{(1)} = P_{\max}^{(3)}.$$

Therefore, only for comparatively large specimen sizes can the tensile strength σ_u be obtained as $\sigma_u = \sigma_f$. With the usual laboratory specimens, an apparent strength higher than the true one is always found.

The maximum loading capacity $P_{\max}^{(1)}$ of initially cracked specimens according to the cohesive crack model is obtained from the $P - \delta$ diagrams in figs. 10 and 11. On the other hand, the maximum loading capacity $P_{\max}^{(2)}$ according to LEFM can be derived from the following formula:

$$(23) \quad P_{\max}^{(2)} = (K_{IC} t b^{3/2}) [l f(a_0/b)]^{-1}$$

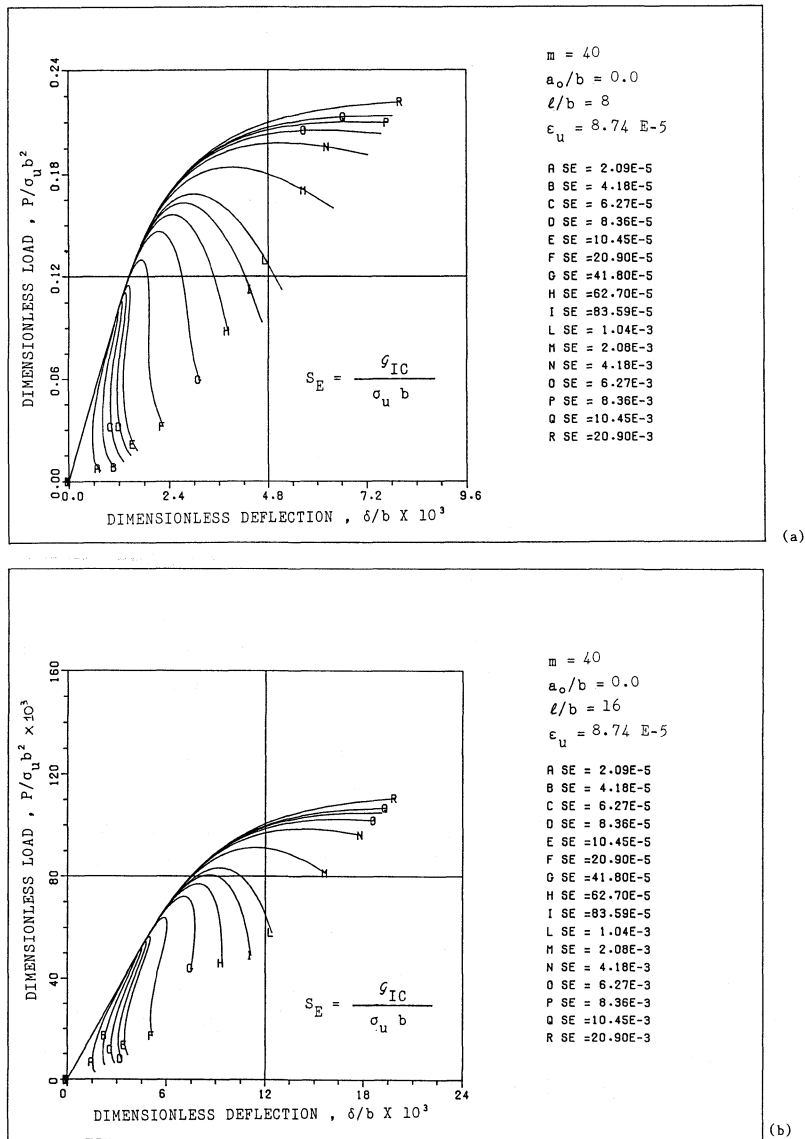


Fig. 12. - Dimensionless load-deflection response of an initially uncracked specimen, by varying the brittleness number, $s_E = G_{IC}/\sigma_u b = \omega_c/2b$, between 2×10^{-5} and 2×10^{-2} . (a) $l/b = 8$; (b) $l/b = 16$.

with the shape-function f given by:

$$f(a_0/b) = 2.9(a_0/b)^{1/2} - 4.6(a_0/b)^{3/2} + 21.8(a_0/b)^{5/2} - 37.6(a_0/b)^{7/2} + 38.7(a_0/b)^{9/2},$$

and the critical value of stress-intensity factor K_{IC} computed according to the well-known relationship:

$$(24) \quad K_{IC} = \sqrt{G_{IC} E}.$$

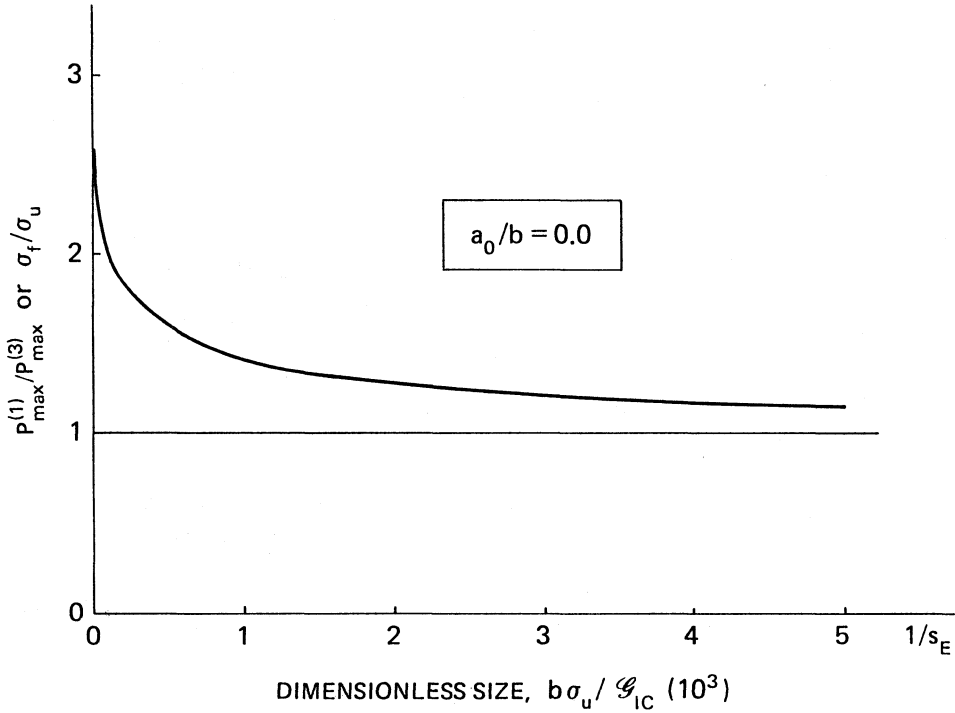


Fig. 13. – Decrease of the apparent ultimate tensile strength σ_f , by increasing the specimen size.

Eventually, a simple ultimate strength analysis on the centre-line with the assumption of a butterfly stress variation through the ligament, provides:

$$(25) \quad P_{\max}^{(3)} = 2\sigma_u t(b - a_0)^2/3l.$$

The values of the ratios $P_{\max}^{(1)}/P_{\max}^{(2)}$ and $P_{\max}^{(3)}/P_{\max}^{(2)}$ are reported as functions of the inverse of the brittleness number s_E in fig. 14. The ratio $P_{\max}^{(1)}/P_{\max}^{(2)}$ may also be regarded as the ratio of the fictitious fracture toughness (given by the non-linear maximum load) to the true fracture toughness (considered as a material constant).

It is evident that, for high s_E numbers, the ultimate strength collapse is a more critical condition than that of LEFM ($P_{\max}^{(3)} < P_{\max}^{(2)}$), as well as the results of the cohesive crack model tend to those of LEFM for low s_E values:

$$(26) \quad \lim_{s_E \rightarrow 0} P_{\max}^{(1)} = P_{\max}^{(2)}.$$

5. LIMIT-CONDITION FOR THE STRUCTURAL BRITTLENESS

When the brittleness number $s_E \rightarrow 0$, $P_{\max}^{(1)} \approx P_{\max}^{(2)}$ and eqs. (23) and (24) provide:

$$(27) \quad \mathcal{G}_{IC} = P_{\max}^2 \lambda^2 f^2(a_0/b)(bt^2E)^{-1}.$$

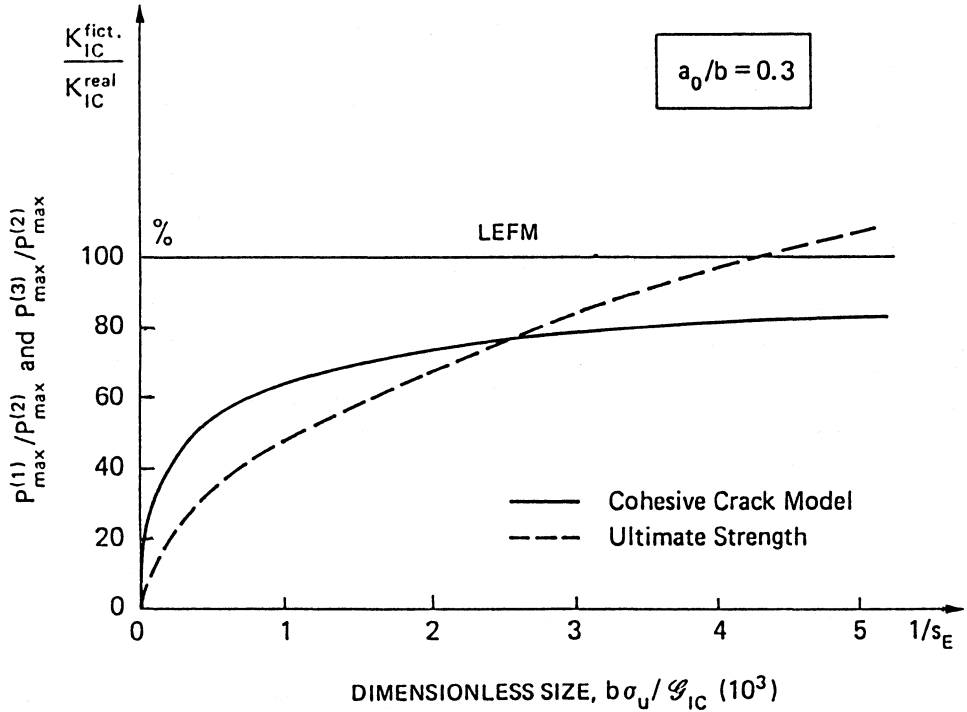


Fig. 14. – Increase of the fictitious fracture toughness $K_{IC}^{fict.}$, by increasing the specimen size ($a_0/b = 0.3$).

On the other hand, the deflection is given by:

$$(28) \quad \delta / \varepsilon_u b^2 = (Pl / \sigma_u t b^2) [\lambda^3 / 4 + (3/2) \lambda^2 g(a_0/b)],$$

with [17]

$$g(a/b) = (a/b)^2 (1 - a/b)^{-2} \{ 5.58 - 19.57(a/b) + 36.82(a/b)^2 - 34.94(a/b)^3 + 12.77(a/b)^4 \},$$

and $\varepsilon_u = \sigma_u / E$.

Since eq. (28) is valid also at the maximum load, eq. (27) is transformed as follows:

$$(29) \quad \mathcal{G}_{IC}(b - a_0) t = (P_{\max} \delta_{\max} / 2) 2 f^2(a_0/b) (1 - a_0/b) [\lambda / 4 + (3/2) g(a_0/b)]^{-1}.$$

If *Brittleness* is defined as the ratio of the elastic energy contained in the body at the maximum load to the energy which can be dissipated in the body, it results to be a function of beam slenderness and initial crack depth (fig. 15):

$$(30) \quad \text{Brittleness} = (P_{\max} \delta_{\max} / 2) [\mathcal{G}_{IC}(b - a_0) t]^{-1} = \\ = [\lambda / 4 + (3/2) g(a_0/b)] [2(1 - a_0/b) f^2(a_0/b)]^{-1}.$$

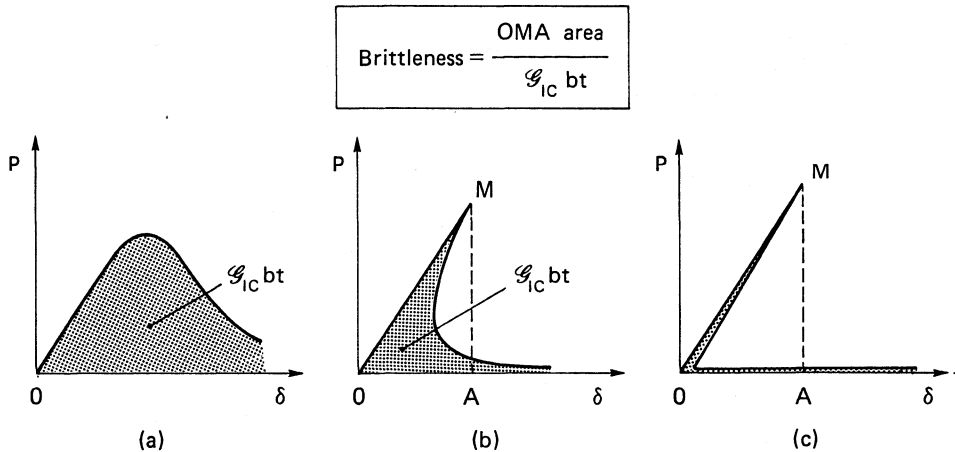


Fig. 15. - Load-deflection diagrams for an initially uncracked beam ($a_0 = 0$): (a) small, (b) intermediate, (c) large size.

When the beam is initially uncracked, *i.e.*, $a_0/b = 0$, the brittleness tends to infinity and the softening branch is coincident with the elastic one (fig. 15c). On the other hand, when the initial crack length is different from zero, *i.e.*, $a_0 \neq 0$, the brittleness tends to the finite value in eq. (30) for the size-scale tending to infinity. In this case, the softening branch is always distinct from the elastic one, so that ultimate elastic energy and energy dissipated by fracture are infinite quantities of the same rank.

ACKNOWLEDGEMENTS

Some of the numerical results reported in the present paper were obtained in a joint research program between ENEL-CRIS-Milano and the University of Bologna.

The Department of Public Education (M.P.I.) is acknowledged for the financial support provided to the present research.

REFERENCES

- [1] G. I. BARENBLATT, *The formation of equilibrium cracks during brittle fracture. General ideas and hypotheses. Axially-symmetric cracks.* J. Appl. Math. Mech., 23, 1959, 622-636.
- [2] Z. P. BAZANT, *Instability, ductility and size effect in strain-softening concrete.* Journal of the Engineering Mechanics Division ASCE, 102, 1976, 331-344.
- [3] B. A. BILBY - A. H. COTTRELL - K. H. SWINDEN, *The spread of plastic yield from a notch.* Proc. R. Soc., A272, 1963, 304-314.
- [4] L. BIOLZI - S. CANGIANO - G. P. TOGNON - A. CARPINTERI, *Snap-back softening instability in high strength concrete beams.* SEM-RILEM International Conference on Fracture of Concrete and Rock (Houston, Texas, June 17-19, 1987), S.P. Shah and S.E. Swartz (eds.), in press.
- [5] A. CARPINTERI, *Notch sensitivity in fracture testing of aggregative materials.* Eng. Fracture Mech., 16, 1982, 467-481.
- [6] A. CARPINTERI, *Application of fracture mechanics to concrete structures.* J. Struc. Div. (A.S.C.E.), 108, 1982, 833-848.
- [7] A. CARPINTERI, *Statistical strength variation in materials with a random distribution of defects.* Università di Bologna, Istituto di Scienza delle Costruzioni, 73, Bologna 1983.

- [8] A. CARPINTERI, *Interpretation of the Griffith instability as a bifurcation of the global equilibrium*. NATO Advanced Research Workshop on *Application of Fracture Mechanics to Cementitious Composites* (Evanston, Illinois, September 4-7, 1984), S. P. Shah (ed.), Martinus Nijhoff, 1985, 284-316.
- [9] D. S. DUGDALE, *Yielding of steel sheets containing slits*. J. Mech. Phys. Solids, 8, 1960, 100-104.
- [10] C. FAIRHURST - J. A. HUDSON - E. T. BROWN, *Optimizing the control of rock failure in servo-controlled laboratory tests*. Rock Mechanics, 3, 1971, 217-224.
- [11] A. HILLERBORG - M. MODEER - P. E. PETERSSON, *Analysis of crack formation and crack growth in concrete by means of fracture mechanics and finite elements*. Cement and Concrete Research, 6, 1976, 773-782.
- [12] G. MAIER, *On the unstable behaviour in elastic-plastic beams in flexure (in Italian)*. Istituto Lombardo, Accademia di Scienze e Lettere, Rendiconti, Classe di Scienze (A), 102, 1968, 648-677.
- [13] J. R. RICE, *A path independent integral and the approximate analysis of strain concentration by notches and cracks*. J. Appl. Mech., 35, 1968, 379-386.
- [14] K. ROKUGO - S. OHNO - W. KOYANAGI, *Automatical measuring system of load-displacement curves including post-failure region of concrete specimens*. International Conference on *Fracture Mechanics of Concrete* (Lausanne, Switzerland, October 1-3, 1985). In: F. H. Wittmann (ed.), *Fracture Toughness and Fracture Energy of Concrete*. Elsevier, Amsterdam 1986, 403-411.
- [15] J. G. ROTS - D. A. HORDIJK - R. DE BORST, *Numerical simulation of concrete fracture in direct tension*. Fourth Intern. Conf. on *Numerical Methods in Fracture Mechanics* (San Antonio, Texas, March 23-27, 1987), Pineridge Press, 1987, 457-471.
- [16] H. SCHREYER - Z. CHEN, *One-dimensional softening with localization*. Journal of Applied Mechanics, 53, 1986, 791-797.
- [17] H. TADA - P. PARIS - G. IRWIN, *The Stress Analysis of Cracks Handbook*. Del Research Corporation, St. Louis (Missouri) 1963, 2.16-17.
- [18] M. P. WNUK, *Quasi-static extension of a tensile crack contained in a viscoelastic-plastic solid*. Journal of Applied Mechanics, 41, 1974, 234-242

Dipartimento di Ingegneria Strutturale - Politecnico di Torino
Corso Duca degli Abruzzi, 24 - 10129 TORINO